Connection between effective-range expansion and nuclear vertex constant or asymptotic normalization coefficient

R. Yarmukhamedov*
Institute of Nuclear Physics, Uzbekistan Academy of Sciences, 100214 Tashkent, Uzbekistan

D. Baye†
Physique Quantique, CP165/82, and Physique Nucléaire Théorique et Physique Mathématique, CP 229, Université Libre de Bruxelles (ULB), B-1050 Bruxelles, Belgium

(Received 26 January 2011; published 5 August 2011)

Explicit relations between the effective-range expansion and the nuclear vertex constant or asymptotic normalization coefficient (ANC) for the virtual decay $B \to A + a$ are derived for an arbitrary orbital momentum together with the corresponding location condition for the $(A + a)$ bound-state energy. They are valid both for the charged case and for the neutral case. Combining these relations with the standard effective-range function up to order six makes it possible to reduce to two the number of free effective-range parameters if an ANC value is known from experiment. Values for the scattering length, effective range, and form parameter are determined in this way for the $^{16}\mathrm{O} + p$, $\alpha + t$, and $\alpha + {}^{3}\mathrm{He}$ collisions in partial waves where a bound state exists by using available ANCs deduced from experiments. The resulting effective-range expansions for these collisions are valid up to energies larger than 5 MeV.

DOI: 10.1103/PhysRevC.84.024603 PACS number(s): 03.65.Nk, 03.65.Ge, 25.40.Cm, 25.55.Ci

I. INTRODUCTION

The effective-range expansion provides a model-independent description of a low-energy phase shift in a given partial wave for the Aa scattering [1–3]. Nevertheless, a lot of ambiguity occurs in the determination of the coefficients of this expansion. Several sets of parameters can describe equally well the low-energy phase shifts. One possibility for removing this ambiguity lies in a consistent description of the low-energy scattering of two particles and of the fundamental characteristics of a two-body $(A + a)$ weakly bound state composed of these two particles [4–7]. The essential quantities required for such a description are the binding energy of this state and its nuclear vertex constant (NVC) or its asymptotic normalization coefficient (ANC) which determines the amplitude of the tail of the bound-state wave function in the two-particle channel. The introduction of these two experimental values into a phase-shift analysis performed with the effective-range expansion could allow one to reduce the ambiguity for the first coefficients of this expansion. Moreover, the first coefficients obtained in such a way should be helpful to test the validity of microscopic models [8] or to constrain properties of two-body potentials.

In Refs. [4–7], different forms of the ANC for the $A + a \to B$ vertex with two charged particles (A and a) and an arbitrary orbital momentum l were derived for the standard effective-range function. For example, two expressions are derived in Ref. [6] for the ANC, one for the neutral case and another one for the charged case.

In the present work, the results of Ref. [6] are generalized for an effective-range function which is valid for both the charged and the neutral cases. Combining this expression with the bound-state condition on the effective-range expansion and taking into account the additional information about experimental values of the ANC for $A + a \to B$ makes it possible to reduce the number of free parameters in the expansion to two in the effective-range function restricted up to order six in the momentum k.

As applications, we consider the $^{16}\mathrm{O} + p$, $\alpha + t$, and $\alpha + {}^{3}\mathrm{He}$ collisions for which experimental ANC values for the virtual decays $^{16}\mathrm{O} + p \to {}^{17}\mathrm{F}$, $\alpha + t \to {}^{7}\mathrm{Li}$, and $\alpha + {}^{3}\mathrm{He} \to {}^{7}\mathrm{Be}$, respectively, are known. By experimental ANC values, we mean values indirectly determined from an analysis of experimental data. The values of the effective-range expansion parameters obtained in such a way should be reliable.

In Sec. II, the explicit expression for the nuclear vertex constant (or the respective ANC) for the virtual decay $B \to A + a$ with two charged particles A and a and an arbitrary relative angular momentum are derived for the standard effective-range expansion. Detailed expressions restricted to terms up to k^6 are established. They are also valid for the neutral case. The results of the application of these expressions to various concrete scatterings of light nuclei, for which the corresponding ANCs are known, are presented in Sec. III. A conclusion is given in Sec. IV.

II. EFFECTIVE-RANGE EXPANSION AND NUCLEAR VERTEX CONSTANT

Let us consider two particles A and a of charges Z_A and Z_a, respectively, with a reduced mass μ. Let k be the relative momentum of particles A and a. The center-of-mass energy is $E = k^2/2\mu$ and the dimensionless Sommerfeld parameter is $\eta = Z_A Z_a e^2 \mu / k$. Let us denote by l (j) the orbital (total) angular momentum of the relative motion of these particles,

*rakhim@inp.uz
†dbaye@ulb.ac.be

by δ_{lj} the Coulomb modified nuclear phase shift, and by $\sigma_l = \arg\Gamma(l+1+i\eta)$ the Coulomb phase shift for the Aa scattering. Everywhere we use the unit $\hbar = 1$.

The partial scattering matrix or S matrix S_{lj} in the presence of both a Coulomb and a nuclear interaction is determined by [9]

$$S_{lj} = e^{2i(\delta_{lj}+\sigma_l)} = \frac{\Gamma(l+1+i\eta)}{\Gamma(l+1-i\eta)}\,\frac{\cot\delta_{lj}+i}{\cot\delta_{lj}-i}. \tag{1}$$

Since this S matrix has a rather complicated analytical structure in the complex E plane, it is useful to introduce a function with simpler analytical properties [10,11],

$$F_{lj}(k^2) = \frac{e^{2i\delta_{lj}}-1}{2i}\,\frac{l!^2 e^{2i\sigma_l}e^{\pi\eta}}{k^{2l+1}\Gamma^2(l+1+i\eta)}. \tag{2}$$

This function can be rewritten in the form

$$F_{lj}(k^2) = \frac{1}{k^{2l+1}C_0^2(\eta)D_l(\eta)(\cot\delta_{lj}-i)}, \tag{3}$$

with the definitions

$$C_0^2(\eta) = \frac{2\pi\eta}{e^{2\pi\eta}-1}, \qquad D_{l>0}(\eta) = \prod_{n=1}^{l}(1+\eta^2/n^2). \tag{4}$$

For the s wave ($l=0$), the factor $D_0(\eta)$ in Eq. (3) is unity. The function D_l is related to the function w_l used in Ref. [6] by $D_l = \eta^{2l}w_l/l!^2$. While w_l does not require a special treatment of $l=0$ and is very convenient to study the limit $E\to 0$ [12], D_l does not require a separate treatment of the neutral case $\eta = 0$.

The effective-range function is defined as

$$K_{lj}(k^2) = \frac{1}{F_{lj}(k^2)} + 2\eta D_l(\eta)H(\eta)k^{2l+1} \tag{5}$$

$$= k^{2l+1}D_l(\eta)\big[C_0^2(\eta)\cot\delta_{lj} + 2\eta h(\eta)\big]. \tag{6}$$

Here

$$H(\eta) = \psi(i\eta) - \ln(i\eta) + 1/2i\eta = h(\eta) + \frac{i}{2\eta}C_0^2(\eta), \tag{7}$$

where ψ is the digamma function [13],

$$h(\eta) = -\gamma + \eta^2\sum_{n=1}^{\infty}\frac{1}{n(n^2+\eta^2)} - \ln\eta, \tag{8}$$

and $\gamma = 0.57721\ldots$ is Euler's constant. When η is real, $h(\eta)$ is the real part of $H(\eta)$.

The Coulomb-nuclear partial elastic-scattering amplitudes are defined as

$$M_{lj}(E) = \frac{i\pi}{\mu k}\,e^{2i\sigma_l}(e^{2i\delta_{lj}}-1). \tag{9}$$

They are related to the $F_{lj}(k^2)$ function by Eq. (2) and thus to the effective-range function $K_{lj}(k^2)$ in Eq. (5) by

$$M_{lj}(E) = -\frac{2\pi}{\mu}\,\frac{k^{2l}\Gamma^2(l+1+i\eta)e^{-\pi\eta}}{l!^2[K_{lj}(k^2) - 2\eta D_l(\eta)H(\eta)k^{2l+1}]}. \tag{10}$$

For negative energies $E=-\varepsilon$, where $\varepsilon>0$ is the binding energy of the bound state of nucleus B in the $(A+a)$ channel, bound states correspond to poles of the scattering partial S_{lj} matrix (or the partial amplitude M_{lj}) on the positive imaginary k axis (or the negative E axis) [11]. Let $k=i\kappa$ be the location of such a pole, where $\kappa = \sqrt{2\mu\varepsilon}$. According to Ref. [14], it follows from Eqs. (9) and (3) that this bound state corresponds to a zero of $F_{lj}^{-1}(-\kappa^2)$. Hence, from the denominator in Eq. (10), one obtains

$$(-1)^l\kappa^{2l+1} = -\frac{K_{lj}(-\kappa^2)}{J_l(\eta_B)}, \tag{11}$$

where $\eta_B = Z_A Z_a e^2\mu/\kappa$ is the Sommerfeld parameter for the $(A+a)$ bound state and the real function $J_l(\eta_B)$ is defined by

$$J_l(\eta_B) = -2\eta_B D_l(-i\eta_B)H(-i\eta_B), \tag{12}$$

with

$$H(-i\eta_B) = \mathrm{Re}\,h(-i\eta_B) - \tfrac{1}{2}\pi\cot\pi\eta_B. \tag{13}$$

Equation (11) is the pole-location condition.

According to Ref. [15], the residue of the partial amplitude $M_{lj}(E)$ at the pole $E=-\varepsilon$ $(k=i\kappa)$ is expressed in terms of the NVC G_{lj} for the virtual decay $B\to A+a$ as

$$\mathrm{res}\,M_{lj}(E) = \lim_{E\to-\varepsilon}(E+\varepsilon)M_{lj}(E) = G_{lj}^2. \tag{14}$$

Alternatively, the NVC can be obtained from the scattering matrix S_{lj} through the relation

$$\mathrm{res}\,S_{lj}(E) = \frac{\mu\kappa}{\pi}\mathrm{res}\,M_{lj}(E). \tag{15}$$

Combining Eqs. (1), (9), (10), and (14), one obtains

$$G_{lj} = i^{l+\eta_B}\sqrt{\frac{2\pi}{\mu}}\,\frac{\kappa^l\Gamma(l+1+\eta_B)}{l!}\left[-\left.\frac{dF_{lj}^{-1}(k^2)}{dE}\right|_{E=-\varepsilon}\right]^{-1/2}. \tag{16}$$

Differentiating function $F_{lj}^{-1}(k^2)$ determined from Eqs. (9) and (10) leads for $E=-\varepsilon$ $(k=i\kappa)$ to the explicit expression for the NVC,

$$G_{lj}^2 = (-1)^l e^{i\pi\eta_B}\frac{2\pi}{\mu^2}\,\frac{\kappa^{2l+1}\Gamma^2(l+1+\eta_B)}{l!^2} \times\left[(-1)^l\kappa^{2l}f_l(\eta_B) - \frac{\kappa}{\mu}\left.\frac{dK_{lj}(k^2)}{dE}\right|_{E=-\varepsilon}\right]^{-1}, \tag{17}$$

where

$$f_l(\eta_B) = D_l(-i\eta_B)\left\{\left(\frac{\pi\eta_B}{\sin\pi\eta_B}\right)^2 - 2\eta_B\left[\tilde{h}(\eta_B) + 2(1-\delta_{l0})H(-i\eta_B)\left(l + \sum_{n=1}^{l}\frac{\eta_B^2}{n^2-\eta_B^2}\right)\right]\right\}, \tag{18}$$

and

$$\tilde{h}(\eta_B) = -\left[\eta\frac{dh}{d\eta}\right]_{\eta=-i\eta_B} = 1 + 2\eta_B^2\sum_{n=1}^{\infty}\frac{1}{n\left(n^2-\eta_B^2\right)} + 2\eta_B^4\sum_{n=1}^{\infty}\frac{1}{n\left(n^2-\eta_B^2\right)^2}. \tag{19}$$

Equations (11) and (17) are quite general. We now particularize them to low binding and scattering energies by using Taylor expansions of the effective-range function $K_{lj}(k^2)$ for $k^2 \to 0$ and we then keep terms up to k^6 in this expansion,

$$K_{lj}(k^2) \approx -\frac{1}{a_{lj}} + \frac{r_{lj}}{2}k^2 - P_{lj}r_{lj}^3k^4 + Q_{lj}k^6, \qquad (20)$$

where the scattering length a_{lj} is in fm^{2l+1}, the effective range r_{lj} is in fm^{-2l+1}, the form parameter P_{lj} is in fm^{4l}, and the sixth-order coefficient Q_{lj} is in fm^{-2l+5}. In this approximation, Eqs. (11) and (17) can be reduced to the forms

$$(-1)^l\kappa^{2l+1} \approx \frac{1/a_{lj} + \frac{1}{2}r_{lj}\kappa^2 + P_{lj}r_{lj}^3\kappa^4 + Q_{lj}\kappa^6}{J_l(\eta_B)} \qquad (21)$$

and

$$G_{lj}^2 \approx (-1)^l e^{i\pi\eta_B}\frac{2\pi}{\mu^2}\frac{\kappa^{2l+1}\Gamma^2(l+1+\eta_B)}{l!^2\mathcal{B}_l(\kappa,\eta_B;r_{lj},P_{lj},Q_{lj})}, \qquad (22)$$

where

$$\mathcal{B}_l(\kappa,\eta_B;r_{lj},P_{lj},Q_{lj}) = (-1)^l\kappa^{2l}f_l(\eta_B) - r_{lj}\kappa - 4P_{lj}r_{lj}^3\kappa^3 - 6Q_{lj}\kappa^5. \qquad (23)$$

It should be noted that, for the case $P_{lj} = Q_{lj} = 0$, Eqs. (22) and (21) coincide with Eq. (31) of Ref. [4] and Eq. (25) of Ref. [5], respectively, if the comments made in Ref. [5] are taken into account. The normalization for the partial amplitude (22) differs from that chosen in Ref. [4] by the Coulomb-phase multiplicative factor $e^{2i\sigma_l}$. The allowance of this factor in the corresponding expressions of Ref. [4] results in the replacement of the factor $K(\eta_B)$, entering in the numerator of the right-hand side of Eqs. (31) and (34) of Ref. [4], by the factor $\Gamma^2(l_B+1+\eta_B)/(l_B!)^2D_{l_B}(-i\eta_B)$, where $l_B = l$.

Besides, the general equations, Eqs. (11) and (17), or the approximate equations, Eqs. (21) and (22), are valid both for the charged case and for the neutral one since $f_l(0) = 2l+1$ and $J_l(0) = 1$. In contrast, the approximate relations (17) and (18) of Ref. [6] are derived separately for the charged and neutral cases, respectively, for $P_{lj} = Q_{lj} = 0$.

In the two-body potential model, the ANC C_{lj} for $A + a \to B$ determines the amplitude of the tail of the B-nucleus bound-state wave function in the $(A+a)$ channel. The ANC is related to the NVC G_{lj} for the virtual decay $B \to A + a$ by [15]

$$G_{lj} = -i^{l+\eta_B}\frac{\sqrt{\pi}}{\mu}C_{lj}, \qquad (24)$$

where the combinatorial factor taking into account the nucleon identity is absorbed in C_{lj}. The numerical value of the ANC depends on the specific model used to describe the wave functions of the A, a, and B nuclei [16]. Hence, the proportionality factor in Eq. (24), which relates NVC and ANC, depends on the choice of nuclear model [16]. But, as noted in Ref. [16], the NVC G_{lj} is a more fundamental quantity than the ANC C_{lj} since the NVC is determined in a model-independent way by Eq. (14) as the residue of the partial amplitude of the Aa elastic scattering at the pole $E = -\varepsilon$.

Using Eqs. (22) and (24), one obtains

$$C_{lj}^2 = \frac{2\kappa^{2l+1}\Gamma^2(l+1+\eta_B)}{l!^2\mathcal{B}_l(\kappa,\eta_B;r_{lj},P_{lj},Q_{lj})}. \qquad (25)$$

As seen from Eq. (23), the NVC or ANC in the effective-range approximation given by Eq. (22) or (25) is expressed through the binding energy ϵ and the effective-range parameters r_{lj}, P_{lj}, and Q_{lj}.

In the absence of Coulomb interaction ($\eta_B = 0$), Eq. (25) can be reduced to

$$C_{lj}^2 = \frac{2\kappa^{2l+1}}{(-1)^l(2l+1)\kappa^{2l} - r_{lj}\kappa - 4P_{lj}r_{lj}^3\kappa^3 - 6Q_{lj}\kappa^5}, \qquad (26)$$

where r_{lj}, P_{lj}, and Q_{lj} are the effective-range parameters for the purely strong interaction. Equation (26) for $l = 0$ and $P_{lj} = Q_{lj} = 0$ coincides with formula (3.12) of Sec. 3 of Chap. 3 of Ref. [17] obtained for the s wave.

It should be noted that Eqs. (21), (22), (25), and (26) can also be applied for resonant states of nucleus B [7]. In this case, the binding energy ε should be replaced by $-E_r + i\Gamma/2$, where E_r and Γ are the energy and width of the resonant state of B in the $(A+a)$ channel, respectively.

Equations (21) and (25) can be used for the analysis of an experimental phase shift for the Aa scattering at low energies if a weakly bound state exists in the lj partial wave and if a value of the ANC is known. In this case, a determination of the effective-range coefficients in the sixth-order approximation (20) makes it possible to reduce the number of parameters to two. For example, Eqs. (21) and (22) can be used to express the r_{lj} and P_{lj} parameters through the a_{lj} and Q_{lj} ones, as well as the ANC C_{lj}, as

$$r_{lj} = \frac{2\kappa^{2l}\Gamma^2(l+1+\eta_B)}{l!^2C_{lj}^2} - \frac{4}{\kappa^2 a_{lj}} + 2Q_{lj}\kappa^4 + (-1)^l\kappa^{2l-1}[4J_l(\eta_B) - f_l(\eta_B)] \qquad (27)$$

and

$$r_{lj}^3\kappa^4P_{lj} = -\frac{\kappa^{2l+2}\Gamma^2(l+1+\eta_B)}{l!^2C_{lj}^2} + \frac{1}{a_{lj}} - 2Q_{lj}\kappa^6 + (-1)^l\kappa^{2l+1}\left[\frac{1}{2}f_l(\eta_B) - J_l(\eta_B)\right]. \qquad (28)$$

By inserting Eqs. (27) and (28) in the right-hand side of Eq. (20), the truncated effective-range function $K_{lj}(k^2)$ given by Eq. (20) can be reduced to the form

$$K_{lj}(k^2) \approx -\frac{1}{a_{lj}}\left(\frac{k^2+\kappa^2}{\kappa^2}\right)^2 + Q_{lj}k^2(k^2+\kappa^2)^2 + \frac{\kappa^{2l-2}\Gamma^2(l+1+\eta_B)}{l!^2C_{lj}^2}k^2(k^2+\kappa^2) - (-1)^l\kappa^{2l-3} \times \left[\frac{1}{2}f_l(\eta_B)(k^2+\kappa^2) - J_l(\eta_B)(k^2+2\kappa^2)\right]k^2. \qquad (29)$$

Equations (6), (25), and (29) make it possible to find a_{lj} and Q_{lj} if the scattering phase shift δ_{lj} and the ANC C_{lj} are replaced by some experimental phase shift at a low energy and

an experimental ANC value, respectively. The values of the a_{lj} and Q_{lj} parameters found in such a way can be used for determining the r_{lj} and P_{lj} parameters with Eqs. (27) and (28).

III. APPLICATIONS

Let us now apply these results to typical nuclear collisions. As examples, we consider the $^{16}O + p$, $\alpha + t$, and $\alpha + {}^3He$ collisions since experimental ANC values are known for $^{16}O + p \to {}^{17}F$ [18], $\alpha + t \to {}^7Li$ [4], and $\alpha + {}^3He \to {}^7Be$ [19], respectively. These collisions have been considered in Ref. [8] within a microscopic cluster model, i.e., the generator-coordinate version of the resonating-group method, where a direct calculation of parameters a_{lj}, r_{lj}, and P_{lj} was performed at zero energy. The exchange and spin-orbit parameters of the nucleon-nucleon effective interaction [20] are fitted to the low-energy experimental phase shifts, which are fairly well reproduced. The microscopic phase shifts and the approximate phase shifts calculated with the effective-range expansion truncated at k^4 agree with each other for $E < 5$ MeV. Therefore, for a low-energy phase-shift analysis, Eqs. (6) and (29) can be safely used with $Q_{lj} = 0$.

The information about the values of the ANCs from Refs. [4,18,19] is taken into account. First, a single free parameter, the scattering length a_{lj}, is adjusted by averaging its value obtained from Eqs. (6) and (29) for several experimental phase shifts measured at low energies. Then the r_{lj} and P_{lj} coefficients of the effective-range expansion are deduced from Eqs. (27) and (28). Finally, we compare them with the coefficients obtained with the microscopic calculation of Ref. [8].

A. $^{16}O + p$

Only the $1/2^+$ and $5/2^+$ partial waves possess bound states, at binding energies 0.60 and 0.105 MeV, respectively. Hence we only analyze the experimental $1/2^+$ and $5/2^+$ phase shifts [21] corresponding to the s and d waves. The experimental ANCs for $^{16}O + p \to {}^{17}F(\text{g.s.}; 5/2^+)$ and $^{16}O + p \to {}^{17}F(0.495\ \text{MeV}; 1/2^+)$ are known [18]. The effective-range parameters $a_{s1/2}$ and $a_{d5/2}$, and their uncertainties, are determined from Eqs. (27) and (28) for $Q_{lj} = 0$ with the experimental phase shifts $\delta_{lj}^{\text{exp}}(E)$. Each point plotted in Fig. 1 corresponds to a different energy E. The uncertainties are the averaged square errors found from Eqs. (6) and (29), which include the experimental errors for the cross sections ($\sim$10%) and the uncertainties of the ANCs.

The weighted means of $a_{s1/2}$ and $a_{d5/2}$ and their uncertainties obtained from all the experimental points are given in the first and fourth lines of Table I. The corresponding mean values for the other effective-range parameters r_{lj} and P_{lj} obtained from the scattering lengths with Eqs. (27) and (28) are also presented. Condition (11) is satisfied but it is very sensitive to the accuracy of the effective range r_{lj}. As seen from Fig. 2, the phase shifts obtained with the effective-range expansions calculated by using the parameters deduced in the present work (solid lines in Fig. 2) are in good agreement with the experimental phase shifts [21].

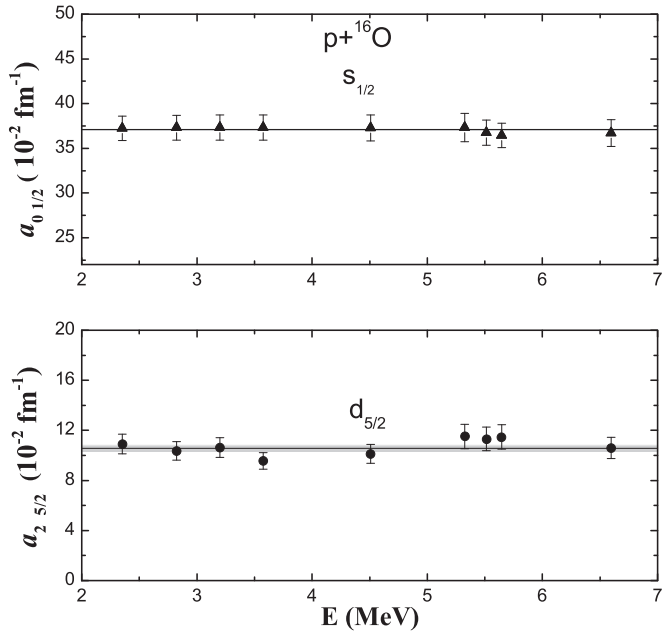

FIG. 1. $^{16}O + p$ scattering lengths for the $s1/2$ (triangles) and $d5/2$ (circles) partial waves. The points are obtained with Eqs. (6) and (29) from experimental phase shifts [21] at various energies. The straight lines and the widths of the bands represent our results for the weighted mean and its uncertainty, respectively.

The effective-range expansion limited at fourth order obtained with the microscopic cluster model of Ref. [8] also provides an accurate reproduction of the same experimental phase shifts for the s wave. For a comparison, the values of the corresponding effective-range parameters deduced in Ref. [8] for the s wave are also given in Table I. They are rather different although they offer an almost identical reproduction of the experimental phase shifts. If one uses the parameters of Ref. [8] (including the energy $\epsilon = 0.65$) to compute the ANC with Eq. (25), one obtains the value 53.2 fm^{-1} presented in the second to the last column, which differs strongly from that recommended in Ref. [18]. One reason for this difference is the

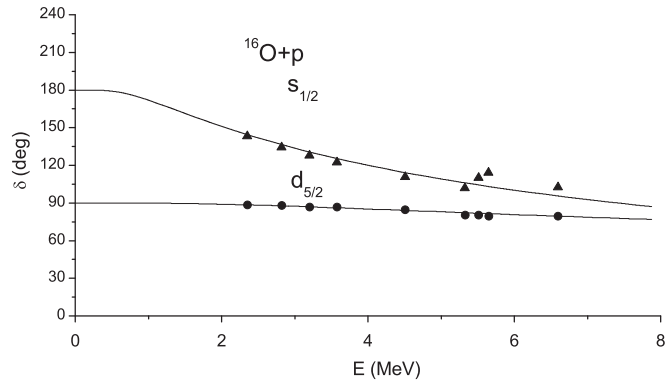

FIG. 2. $s1/2$ and $d5/2$ $^{16}O + p$ phase shifts. The curves display results obtained from the effective-range expansion with parameters from Table I. Triangles ($s_{1/2}$) and circles ($d_{5/2}$) represent experimental values of Ref. [21]. The $d_{5/2}$ phase shifts are shifted by 90° for clarity.

TABLE I. Binding energy ϵ (MeV) and effective-range coefficients for lj partial waves of various collisions: scattering length a_{lj} (fm^{2l+1}), effective range r_{lj} (fm^{-2l+1}), and shape parameter P_{lj} (fm^{4l}). ANCs from the present analysis $(C_{lj}^{\rm eff})^2$ and ANCs deduced from experiment $(C_{lj}^{\rm exp})^2$ (fm^{-1}). In some lines, the ANC is obtained from the effective-range parameters of Ref. [8] (see text).

Collision	l	j	ϵ	a_{lj}	r_{lj}	P_{lj}	$(C_{lj}^{\rm eff})^2$	$(C_{lj}^{\rm exp})^2$
$^{16}O + p$	0	1/2	0.105	3708 ± 48	1.156 ± 0.005	-0.17 ± 0.36	5700	5700 ± 225 [18]
			0.65	815 [8]	1.16 [8]	-0.22 [8]	53.2	
			0.105	3828	1.16 [8]	-0.22 [8]	5850	
	2	5/2	0.60	1057 ± 27	-0.0804 ± 0.007	-365.6 ± 161.7	1.09	1.09 ± 0.11 [18]
$\alpha + t$	1	1/2	1.99	95.13 ± 1.73	-0.238 ± 0.007	39.18 ± 4.90	9.00	9.00 ± 0.90 [4]
			3.75	108.9 [8]	-0.22 [8]	56.99 [8]	7.70	
			1.99	90.1	-0.22 [8]	56.99 [8]	5.43	
	1	3/2	2.47	58.10 ± 0.65	-0.346 ± 0.005	9.86 ± 0.76	12.74	12.74 ± 1.10 [4]
			4.99	72.77 [8]	-0.27 [8]	26.59 [8]	16.47	
			2.47	69.9	-0.27 [8]	26.59 [8]	8.82	
$\alpha + {}^3$He	1	1/2	1.156	413 ± 7	-0.00267 ± 0.0028	$(2.66 \pm 8.39) \times 10^7$	15.9	15.9 ± 1.1 [19]
			2.88	665 [8]	-0.01 [8]	3.56×10^6 [8]	0.28	
	1	3/2	1.587	301 ± 6	-0.0170 ± 0.0026	$(9.69 \pm 4.69) \times 10^4$	23.2	23.2 ± 1.7 [19]
			3.99	253.1 [8]	-0.04 [8]	9212 [8]	4.79	

fact that the microscopic model provides a too large binding energy equal to 0.65 MeV.

To understand this discrepancy, we calculate $C_{s1/2}^2$ with the microscopic $r_{s1/2}$ and $P_{s1/2}$ but now with the exact binding energy 0.105 MeV (see the third line in Table I). The result 5850 fm^{-1} is now close to the experimental value. This is due to the good agreement for the effective range and the form parameter. Introducing this value in the pole condition (11), one obtains the scattering length 3828 fm in good agreement with the value in the first line of Table I. However, a close reproduction of the phase shifts is important. By fitting the exchange parameter in the effective interaction to reproduce the experimental binding energy 0.105 MeV, one obtains a poor reproduction of the experimental phase shifts. The corresponding values $a_{s1/2} = 4673$ fm, $r_{s1/2} = 1.18$ fm, and $P_{s1/2} = -0.23$ obtained in Ref. [8] lead to $(C_{s1/2})^2$ equal to 7142 fm^{-1}. This ANC value is significantly better than the value deduced above from the parameters of Ref. [8] but it is less good than when the phase shifts are fitted.

It is interesting to note that the effective-range expansions lead to very similar low-energy phase shifts because the effective ranges $r_{s1/2}$ are in very good agreement. The important difference between the scattering lengths has very little influence because it is the inverse of this large parameter that appears in the effective-range expansion. However, the parameters of Ref. [8] allow one to reliably estimate the ANC only if the experimental binding energy is used.

Thus, for the $^{16}O + p$ collision, the application of formula (25) together with condition (11) makes it possible to choose a set of effective-range parameters simultaneously describing the fundamental characteristics of the weakly bound states of the ^{17}F nucleus and the $^{16}O + p$ collision in a consistent way.

B. $\alpha + t$ and $\alpha + {}^3$He

For the $\alpha + t$ and $\alpha + {}^3$He collisions, we only consider the $p3/2$ and $p1/2$ partial waves that contain bound states (see the binding energies ϵ in Table I). The scattering lengths obtained as a function of experimental phase shifts [22] for the $p1/2$ and $p3/2$ partial waves of the $\alpha + t$ and $\alpha + {}^3$He collisions are displayed in Figs. 3 and 4, respectively. The experimental ANC values for the ground and first excited states of the ^{7}Li and ^{7}Be nuclei in $\alpha + t \to {}^7$Li and $\alpha + {}^3$He $\to {}^7$Be, respectively, are taken from Refs. [4,19]. The corresponding effective-range parameters are given in Table I.

As seen in Figs. 5 and 6 for both collisions, the fourth-order effective-range expansions with the coefficients obtained

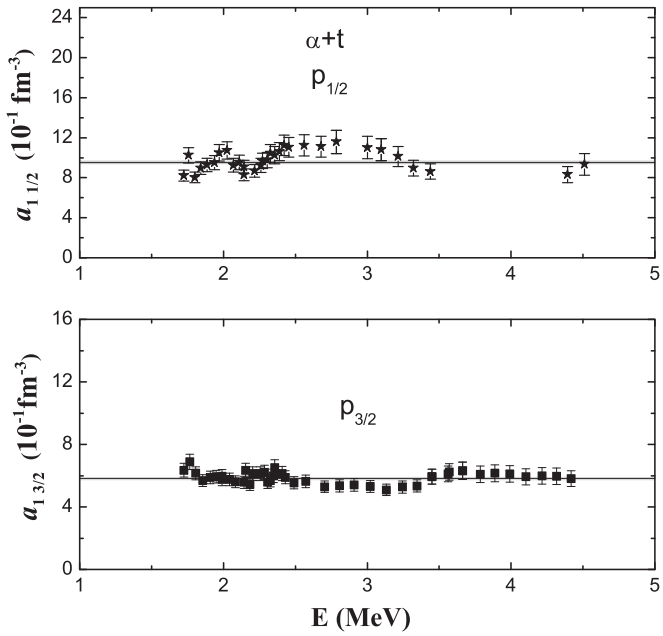

FIG. 3. $\alpha + t$ scattering lengths for the $p1/2$ (stars) and $p3/2$ (squares) partial waves. The points are obtained with Eqs. (6) and (29) from experimental phase shifts [22] at various energies. The straight lines and the widths of the bands represent our results for the weighted mean and its uncertainty, respectively.

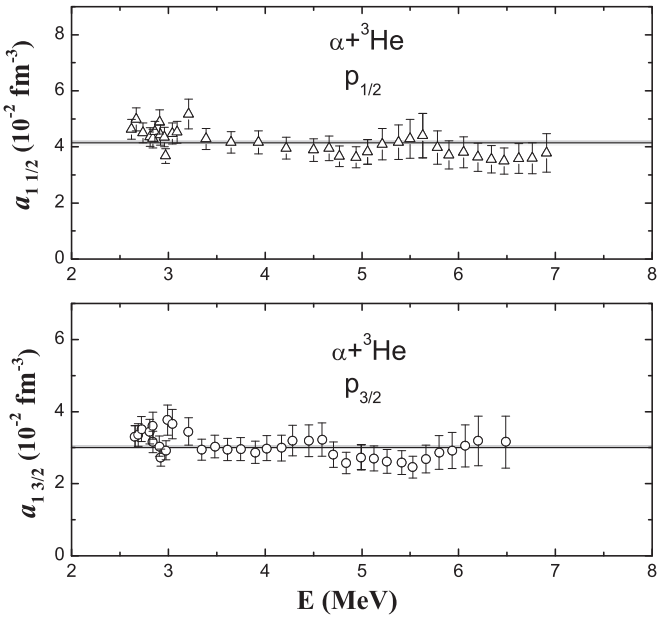

FIG. 4. $\alpha + {}^3$He scattering lengths for the $p1/2$ (triangles) and $p3/2$ (circles) partial waves. See caption of Fig. 3.

in the present work provide good parametrizations of the experimental $p_{1/2}$ and $p_{3/2}$ phase shifts [22] up to at least 5 MeV.

For a comparison, the results for the effective-range parameters obtained in Ref. [8] are presented in Table I. They also reproduce the experimental phase shifts: in fact, the curves are indistinguishable from the present ones. But they give ANC values that differ noticeably from the ANC values of Refs. [4,19] (see the second to the last column in Table I), especially in the $\alpha + {}^3$He case. Here also, the microscopic cluster model provides too large binding energies ϵ for both states of ^{7}Li and ^{7}Be. Hence, the values of the effective-range parameters obtained in Ref. [8] do not satisfy the bound-state energy condition (11). The effective-range parameters obtained in the present work and the ANC values that we use correspond to the experimental bound-state energies and accurately verify condition (11) before rounding.

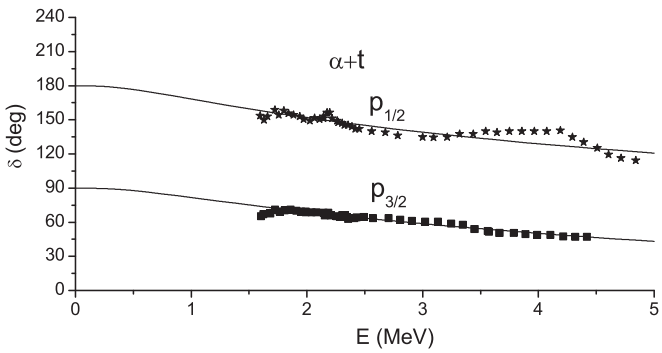

FIG. 5. $p1/2$ and $p3/2$ $\alpha + t$ phase shifts. The curves display results obtained from the effective-range expansion with parameters from Table I. Stars ($p_{1/2}$) and squares ($p_{3/2}$) represent experimental values of Ref. [22]. The $p_{3/2}$ phase shifts are shifted by 90° for clarity.

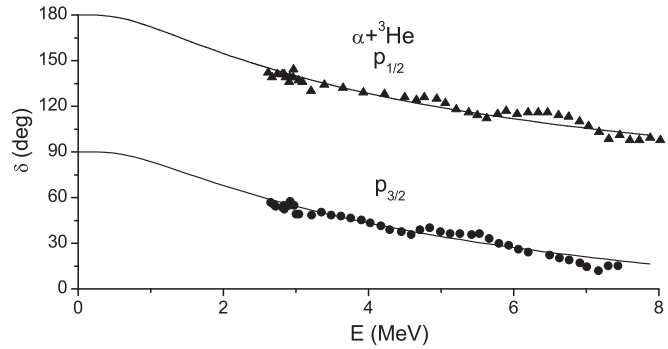

FIG. 6. $p1/2$ and $p3/2$ $\alpha + {}^3$He phase shifts. The curves display results obtained from the effective-range expansion with parameters from Table I. Triangles ($p_{1/2}$) and circles ($p_{3/2}$) represent experimental values of Ref. [22]. The $p_{3/2}$ phase shifts are shifted by 90° for clarity.

In the $\alpha + t$ case, we replace the microscopic binding energy by the experimental ones. Contrary to the $^{16}\mathrm{O} + p$ case, this modification does not improve the agreement with the experimental ANC (see Table I). This can be understood by the fact that the microscopic effective range and form parameter are not very close to the present ones, probably because the error on the binding energy is much larger. Most likely, only a microscopic model reproducing simultaneously the binding energy and phase shifts would overcome this drawback. A similar problem occurs for $\alpha + {}^3$He.

IV. CONCLUSION

Explicit expressions for the NVC and ANC for the virtual decay $B \to A + a$ at an orbital momentum l and the corresponding pole condition for the energy of the bound $(A + a)$ state are derived as a function of the effective-range expansion $K_{lj}(k^2)$. They are valid both for the charged case and for the neutral case. These expressions are particularized for an expansion restricted to terms up to k^6. Combining these expressions with the experimental value of the NVC (or ANC) makes it possible to reduce the number of free parameters in the expansion to two (or to one if the sixth-order parameter Q_{lj} is chosen as zero). This can lead to rather simple parametrizations of phase shifts at low energies when a bound state occurs in the partial wave.

These expressions were also used for an analysis of the experimental phase shifts for the $^{16}\mathrm{O} + p$, $\alpha + t$, and $\alpha + {}^3$He collisions. The obtained coefficients of the effective-range expansions reproduce rather well the low-energy experimental phase shifts. These results can thus be considered as experimental values since they fit consistently the experimental data for both the continuum and a bound state, i.e., the phase shifts and the bound-state energy and ANC.

A comparison with the coefficients of the effective-range expansions obtained in Ref. [8] within a microscopic cluster model has been performed for the same collisions. It is useful for testing their reliability. Despite reproductions of phase shifts of similar quality, a significant disagreement is observed for the scattering length and the deduced ANC. It can be

related to the fact that the microscopic model cannot reproduce simultaneously the phase shifts and the binding energies. With a correct binding energy, the microscopic model allows a good prediction of the ANC for $^{16}O + p$, but not for the other collisions where the error on the energy is much larger. This problem should be solved in future *ab initio* calculations using realistic nucleon-nucleon interactions.

We think that the present results consistent with experiments both for the continuum and for a weakly bound state should be useful to construct nucleon-nucleus and nucleus-nucleus potentials appearing in different nuclear models.

ACKNOWLEDGMENTS

R.Y. was supported in part by the Foundation for Fundamental Research of the Uzbekistan Academy of Science (Grant No FA-F2-F077). D.B. thanks J.-M. Sparenberg for useful discussions. This text presents research results of the Belgian Research Initiative on exotic nuclei (BriX), Program P6/23 on interuniversity attraction poles of the Belgian Federal Science Policy Office. R.Y. acknowledges financial support from this program. He also thanks the theoretical nuclear physics group PNTPM-ULB, where this work was completed, for the hospitality during December 2010.

[1] J. M. Blatt and J. D. Jackson, Phys. Rev. **76**, 18 (1949).
[2] H. A. Bethe, Phys. Rev. **76**, 38 (1949).
[3] M. A. Preston and R. K. Bhaduri, *Structure of the Nucleus* (Addison-Wesley, Reading, MA, 1975).
[4] S. B. Igamov and R. Yarmukhamedov, Nucl. Phys. A **781**, 247 (2007).
[5] S. B. Igamov and R. Yarmukhamedov, Nucl. Phys. A **832**, 346 (2010).
[6] J.-M. Sparenberg, P. Capel, and D. Baye, Phys. Rev. C **81**, 011601(R) (2010).
[7] Yu. V. Orlov, B. F. Irgaziev, and L. I. Nikitina, Phys. At. Nucl. **73**, 757 (2010).
[8] R. Kamouni and D. Baye, Nucl. Phys. A **791**, 68 (2007).
[9] R. G. Newton, *Scattering Theory of Waves and Particles*, 2nd ed. (Springer, New York, 1982).
[10] J. Hamilton, I. Overbö, and B. Tromborg, Nucl. Phys. B **60**, 443 (1973).
[11] H. van Haeringen, J. Math. Phys. **18**, 927 (1977).
[12] D. Baye and E. Brainis, Phys. Rev. C **61**, 025801 (2000).
[13] M. Abramowich and I. A. Stegun, eds., *Handbook of Mathematical Functions* (Dover, New York, 1965).
[14] Z. R. Iwinski, L. Rosenberg, and L. Spruch, Phys. Rev. C **29**, 349 (1984).
[15] L. D. Blokhintsev, I. Borbely, and E. I. Dolinskii, Fiz. Elem. Chastits At. Yadra **8**, 1189 (1977) [Sov. J. Part. Nucl. **8**, 485 (1977)].
[16] L. D. Blokhintsev and V. O. Yeromenko, Yad. Fiz. **71**, 1247 (2008) [Phys. At. Nucl. **71**, 1219 (2008)].
[17] A. I. Baz', Y. B. Zel'dovich, and A. M. Perelomov, *Scattering, Reactions and Decay in Nonrelativistic Quantum Mechanics*, translated from Russian by Z. Lerman (IPST, Jerusalem, 1969).
[18] S. V. Artemov, S. B. Igamov, Q. I. Tursunmakhatov, and R. Yarmukhamedov, Izv. RAN: Seriya Fizicheskaya **73**, 176 (2009) [Bull. Russian Acad. Sci. Phys. **73**, 165 (2009)].
[19] S. B. Igamov, Q. I. Tursunmahatov, and R. Yarmukhamedov, arXiv:0905.2026 [nucl-th].
[20] D. R. Thompson, M. LeMere, and Y. C. Tang, Nucl. Phys. A **286**, 53 (1977).
[21] L. Brown, W. Haeberli, and W. Trächslin, Nucl. Phys. A **90**, 339 (1967).
[22] R. J. Spiger and T. A. Tombrello, Phys. Rev. **163**, 964 (1967).